SINGULAR PERTURBATION APPROACH TO MOVING MASS CONTROL OF BUOYANCY-DRIVEN AIRSHIP IN 3-D SPACE

Wu Xiaotao[1,2], *Claude H Moog*[2], *Hu Yueming*[1]

(1. Automation College, South China University of Technology, Guangzhou, 510640, P. R. China;
2. Nantes Communication and Cybernetics Research Institute, Nantes, 44321, France)

Abstract: The attitude control problem and the guidance problem are solved in 3-D for a buoyancy-driven airship actuated by the combined effects of an internal air bladder which modulates the airship's net weight and of two moving masses which modulate its center of mass. A simple and clear modeling is introduced to derive the 8 degree of freedom (DOF) mathematical model. Nonlinear control loops are derived through maximal feedback linearization with internal stability for both dynamics in the longitudinal plane and in the lateral plane. Based on a singular perturbation approach, the superposition of these two control actions in the longitudinal plane and in the lateral plane is shown to achieve the control of the dynamics in 3-D space. The simulations of the airship tracking specified attitude, moving direction and speed in 3-D space are presented.

Key words: buoyancy-driven; airship; nonlinear control; 3-D; singular perturbation

CLC number: TP2; V1 **Document code**: A **Article ID**: 1005-1120(2011)04-0343-10

INTRODUCTION

Airships are no longer used for passenger transportation, however, they are useful for other purposes, such as surveillance, communication relay, and heavy lift transportation[1-4]. Major countries in the world have independently set up new projects, for instance, the hybrid airship project of Northrop Grumman, Lockheed Martin's project, European ESA-HALE project[3-4], and some others[5-6].

The structure and operating mechanism of a buoyancy-driven airship was explicitly depicted in Ref. [7], which employed an internal air bladder to modulate the airship's net weight while one or more moving mass actuators modulated its center of mass (Figs. 2-3). Through appropriate cycles of its actuators, the airship can navigate with higher efficiency than conventional actuators (diesel or electrical engine, elevator, rudder, etc.). This buoyancy-driven concept was initially conceived by Henry Stommel[8], and it motivated the development of several operational underwater gliders[9-11]. This mechanism was introduced to generate a new-kind airship by Purandare[7].

The physical properties and the longitudinal dynamics of the buoyancy-driven airship was explicitly analyzed in Ref. [7]. For the underwater glider which uses the same mechanism, a complete 8 degree of freedom (DOF) mathematical model was derived in Ref. [9]. Due to the existence of the internal DOF, the dynamics of this mechanical system becomes complex and yields an under-actuated system. Some works are dedicated to analyze the longitudinal dynamics. A linear controller based on linear-quadratic regulator (LQR) was derived in Ref. [9], and Lyapunov approach was used in Ref. [12] for the underwater glider. Based on some simplified special cases, the longitudinal dynamics were analyzed and a nonlinear controller was derived based on a maximal feedback linearization with internal stability in Ref. [13] for the buoyancy-driven airship.

For the modeling of the 8-DOF dynamics of

Foundation item: Supported by the Scholarship Foundation of China Scholarship Council.

Received date: 2010-12-03; **revision received date**: 2011-04-20

E-mail: wuxiaotao@gmail.com

this mechanical system in Refs. [9,12], the system dynamics is described in terms of the total system momentum and the moving masses momentum, which leads to a useless complexity of the modeling. This paper adopts a new view for modeling: the rigid body and the moving masses are two independent subsystems, and the coupling of these two subsystems only consists of a set of a forces and moments. The advantage of this approach is that it makes the model easy to be derived since the modeling of the rigid body of this airship will be similar to that of the conventional airship[14-15]. Another is that it presents the interconnections of this moving masses controlled buoyancy-driven airship.

The attitude and guidance of the airship are controlled by two similar moving masses and the net buoyancy, etc, as shown in Fig. 1. The attitude of the airship is mainly controlled by the position of the moving masses which is represented by $\boldsymbol{r}_p$ in this paper, the guidance which consists of the speed V and two flight path angles mainly depends on the attitude, the net buoyancy, and aerodynamic forces.

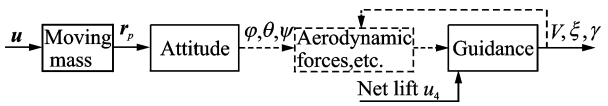

Fig. 1 Structure of buoyancy-driven airship model

The longitudinal dynamics of the buoyancy-driven airship was analyzed in Ref. [13] based on some assumed simplified cases and the maximal feedback linearization approach, and a nonlinear controller was derived for the attitude control and the guidance in longitudinal plane. The lateral dynamics is similar to that of the longitudinal plane, only the parameters differ. By a similar analysis approach as what was done in the longitudinal plane in Ref. [13], a nonlinear controller is derived for the attitude control and the guidance in the lateral plane in this paper. Thus, for both longitudinal and lateral dynamics, nonlinear controllers are derived which solve the maximal linearization problem with internal stability.

To solve the control problem in 3-D space with results derived for 2-D cases, a singular perturbation approach is adopted as a tool to combine the two controllers designed for the longitudinal and lateral planes. In this case, the longitudinal dynamics is assumed to be slow and the lateral dynamics is assumed to be fast. The simulations show that this control scheme is acceptable for the control problem in 3-D space. It is also valid and instrumental for similar mechanical systems, such as underwater gliders and re-entry vehicles[16].

The singular perturbation approach developed is different from the standard singular perturbation approach for the aerial vehicles depicted in Ref. [17]. Usually the problem is split into the attitude control problem and the guidance problem. Here, the singular perturbation method is a tool which allows superposing both control loops for longitudinal and lateral motions.

Some assumptions are made here. In these first results, the theoretical issues are argued and disturbances as the wind, variation of air density or of temperature are not considered.

1 VEHICLE DYNAMICAL MODEL

1.1 Buoyancy-driven airship

The structure and the operating mechanism of an airship driven by moving masses and adjusting weight were explained in Ref. [7]. The basic structure of the airship is shown in Figs. 2-3. The airship hull is inflated with helium and ambient air in two isolated bladders. The internal air bladder is symmetrical and elastic and its mass can be adjusted by a blower and valves. Since the volume of the airship is invariant , the buoyancy of the

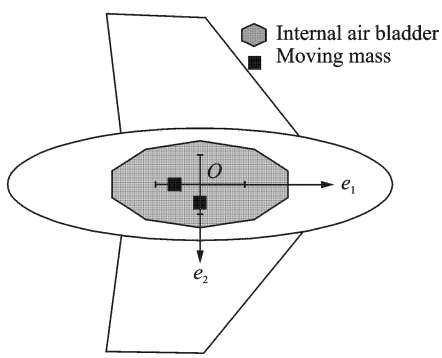

Fig. 2 Top view of airship

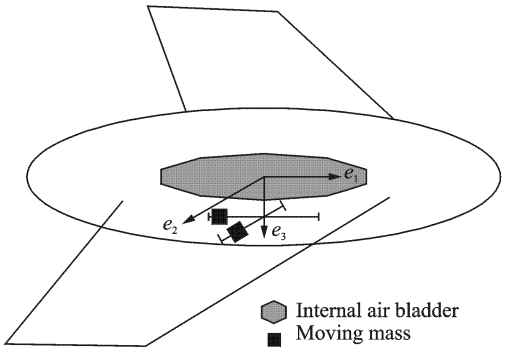

Fig. 3 Side view of airship

airship is constant. By adjusting the mass of internal bladder, the airship will rise or fall down.

There are two moving masses located at the bottom of the airship, and they can move along e_1 and e_2 directions of the body frame. According to the motion of the moving masses, the center of gravity of the airship CG also moves, which leads to the variation of the attitude of the airship.

The airship is also equipped with some fins which help to increase the aerodynamic force, but there is neither rudder nor elevator.

The operating mechanism is briefly described as follows. When releasing air from the air bladder, the mass of the airship reduces, thus, the net lift becomes positive and the airship rises. When the moving mass moves to the $-e_1$ direction, the airship gets a positive pitch angle θ, which yields a forward aerodynamic component force acting on the airship. This component force makes it move forward (the BC segment of Fig. 4). Conversely, when pumping air into the air bladder, the mass of the airship increases, the airship falls down. When the moving mass moves to the $+e_1$ direction, the pitch angle θ becomes negative, which still yields a forward aerodynamic component force. Therefore the airship moves downward and forward (the AB segment of Fig. 4). If the moving mass moves to the sides, the airship will roll. Due to the coupling of roll, pitch and yaw moments, the airship turns to right or left direction.

Two limiting assumptions are made at the outset of building the full non-linear 8-DOF mathematical model for practical reasons:

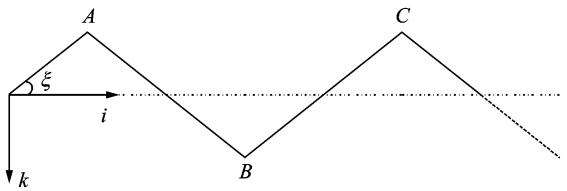

Fig. 4 Typical trajectory in longitudinal plane

(1) The airship forms a rigid body such that aeroelastic effects can be ignored;

(2) The airframe is symmetric about the e_1e_2 plane, and the resulting center of mass of all airship components lies in the center of the volume O, except the two moving masses.

For 8-DOF mathematical model, different from Refs. [9,12] where the airship body and the internal moving masses were viewed as a global system, the rigid body and the moving masses $\overline{m}$ are viewed as independent parts here (as shown in Fig. 5). Thus, the modeling of the conventional airship[14] is referable here. The moving masses are modeled independently. The only coupling between two parts is force u which is considered to be the control.

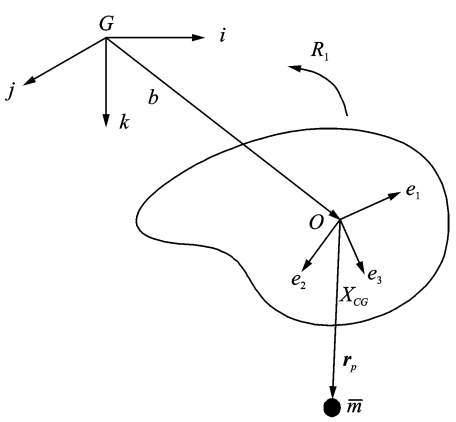

Fig. 5 Rigid airframe and moving mass

1.2 Dynamics of moving mass

As depicted in Fig. 5, the rigid airframe and the moving mass are assumed to be immersed in static atmosphere without disturbance. The velocity of the ballast in the body frame $\boldsymbol{v}_p$ is

$$\boldsymbol{v}_p = \boldsymbol{v} + \dot{\boldsymbol{r}}_p + \Omega \times \boldsymbol{r}_p \tag{1}$$

and the total external force acting on the moving mass is given by

$$\boldsymbol{F}_p = (\overline{m}\boldsymbol{v}_p) \times \Omega + \overline{m}g\boldsymbol{R}_1^{\mathrm{T}}\boldsymbol{k} + \boldsymbol{u} \tag{2}$$

According to Newton's Second Law and Eqs. (1,2), the acceleration of the moving mass is derived as

$$\ddot{\boldsymbol{r}}_p = -\dot{\boldsymbol{v}} - \dot{\boldsymbol{\Omega}} \times \boldsymbol{r}_p - \boldsymbol{\Omega} \times \dot{\boldsymbol{r}}_p + g(\boldsymbol{R}_1^{\mathrm{T}} \boldsymbol{k}) + \frac{1}{\overline{m}}(\overline{m}\boldsymbol{v}_p \times \boldsymbol{\Omega} + \boldsymbol{u}) \tag{3}$$

Note that the mass is only moving in a plane parallel to e_1e_2 here, which means that it cannot move along the e_3 axis and r_{p3} in $\boldsymbol{r}_p$ is constant.

1.3 Dynamics of airframe

The dynamic model of the airframe is stated as

$$\boldsymbol{M}\dot{\boldsymbol{v}} = \boldsymbol{F}_{\mathrm{d}} + \boldsymbol{F}_{\mathrm{a}} + \boldsymbol{F}_{\mathrm{GB}} + \boldsymbol{F}_{\mathrm{I}} \tag{4}$$

$$\boldsymbol{J}\dot{\boldsymbol{\Omega}} = \boldsymbol{M}_{\mathrm{d}} + \boldsymbol{M}_{\mathrm{a}} + \boldsymbol{M}_{\mathrm{GB}} + \boldsymbol{M}_{\mathrm{I}} \tag{5}$$

Each of the components in Eqs. (4-5) is described in the following. Different from the conventional airship[14], there is no propulsion in Eqs. (4-5) since the airship here is driven by the buoyancy.

(1)Linear velocity $\boldsymbol{v}$ and angular velocity $\boldsymbol{\Omega}$

Let the linear velocity vector $\boldsymbol{v}=[v_1,v_2,v_3]^{\mathrm{T}}$ and the angular velocity vector $\boldsymbol{\Omega}=[\Omega_1,\Omega_2,\Omega_3]^{\mathrm{T}}$, all written with respect to the body frame $O\{e_1, e_2, e_3\}$. For the trajectory tracking purpose, $\boldsymbol{v}$ has to be transformed to an inertial frame $G\{i,j,k\}$ by a rotation matrix $\boldsymbol{R}_1$ as

$$\dot{\boldsymbol{b}} = \boldsymbol{R}_1\boldsymbol{v}$$

(2) Mass matrix $\boldsymbol{M}$ and moment of inertia matrix $\boldsymbol{J}$

The mass matrix incorporates all masses and the inertial terms. The inertia of the airship is much more significant due to its large volume/mass ratio in comparison with conventional airplanes. Therefore, the inertia has to be considered.

In case of a rigid body in an ideal fluid with velocity v_i in the direction i, the force acting on the rigid body by the fluid in the direction j is $-m_{ij}\dot{v}_i$ and the parameter m_{ij} is called the added mass. There are 36 added masses for a rigid body in motion[18]. However, only the added masses in the diagonal are considered for simplicity in this research, and $\boldsymbol{M}$ and $\boldsymbol{J}$ are given by

$$\boldsymbol{M} = \mathrm{diag}\{m_1,m_2,m_3\} = \mathrm{diag}\{m_s + m_{11}, m_s + m_{22}, m_s + m_{33}\}$$

$$\boldsymbol{J} = \mathrm{diag}\{J_1,J_2,J_3\} = \mathrm{diag}\{I_x + m_{44}, I_y + m_{55}, I_z + m_{66}\}$$

where m_s is the mass of the airship airframe. I_i are the moments of inertia of the airframe about Oe_1, Oe_2, and Oe_3 respectively, m_{11}, m_{22}, and m_{33} the virtual added masses for e_1, e_2, and e_3 respectively, and m_{44}, m_{55}, and m_{66} the virtual added inertia about Oe_1, Oe_2, and Oe_3 respectively. The method for estimating these virtual masses and inertia was indicated in Refs. [19-20].

(3)Dynamic force $\boldsymbol{F}_{\mathrm{d}}$ and moment $\boldsymbol{M}_{\mathrm{d}}$

The force vector $\boldsymbol{F}_{\mathrm{d}}$ contains the Coriolis force and the centrifugal force of the dynamic model, and $\boldsymbol{M}_{\mathrm{d}}$ contains the moment of the Coriolis force and the centrifugal force. $\boldsymbol{F}_{\mathrm{d}}$ and $\boldsymbol{M}_{\mathrm{d}}$ are given by

$$\boldsymbol{F}_{\mathrm{d}} = \boldsymbol{M}_v \times \boldsymbol{\Omega}$$

$$\boldsymbol{M}_{\mathrm{d}} = \boldsymbol{J}\boldsymbol{\Omega} \times \boldsymbol{\Omega} + \boldsymbol{M}_v \times \boldsymbol{v}$$

(4) Aerodynamic force $\boldsymbol{F}_{\mathrm{a}}$ and moment $\boldsymbol{M}_{\mathrm{a}}$

Different pneumatic pressures are distributed on the surface of a vehicle flying in the atmosphere. The effect of those pneumatic pressures can be represented by aerodynamic force $\boldsymbol{F}_{\mathrm{a}}$ and moment $\boldsymbol{M}_{\mathrm{a}}$ as follows

$$\boldsymbol{F}_{\mathrm{a}} = (X_{\mathrm{a}},Y_{\mathrm{a}},Z_{\mathrm{a}})^{\mathrm{T}}$$

$$\boldsymbol{M}_{\mathrm{a}} = (L_{\mathrm{a}},M_{\mathrm{a}},N_{\mathrm{a}})^{\mathrm{T}}$$

where X_{a}, Y_{a}, and Z_{a} are drag, sideforce, and lift, respectively. L_{a}, M_{a}, and N_{a} are roll moment, pitch moment, and yaw moment, respectively. All of these terms are with respect to the body frame. The explicit forms of $\boldsymbol{F}_{\mathrm{a}}$ and $\boldsymbol{M}_{\mathrm{a}}$ can be found in Ref. [15].

(5)Force $\boldsymbol{F}_{\mathrm{GB}}$ and moments $\boldsymbol{M}_{\mathrm{GB}}$ of the gravity and buoyancy

The composition of the gravity and the buoyancy with respect to the body frame is denoted by $\boldsymbol{F}_{\mathrm{GB}}$

$$\boldsymbol{F}_{\mathrm{GB}} = (m_s - m)g\boldsymbol{R}_1^{\mathrm{T}}\boldsymbol{k} = (m_0 - \overline{m})g\boldsymbol{R}_1^{\mathrm{T}}\boldsymbol{k}$$

It is assumed that the center of gravity of the rigid body locates at point O. So there is no moment involved by m_s and the buoyancy of the airship. In the body frame, the latter moment is

$$\boldsymbol{M}_{\mathrm{GB}} = 0$$

(6)Internal force $\boldsymbol{F}_{\mathrm{I}}$ and moments $\boldsymbol{M}_{\mathrm{I}}$

Since the moving masses are actuated by and fixed to the airframe, there exists a reacting force on the airframe which is a significant difference from the conventional airship and airplane. These interactions $\boldsymbol{F}_{\mathrm{I}}$ and $\boldsymbol{M}_{\mathrm{I}}$ are given by

$$\boldsymbol{F}_{\mathrm{I}} = -\boldsymbol{u}$$

$$\boldsymbol{M}_{\mathrm{I}} = -\boldsymbol{r}_p \times \boldsymbol{u}$$

Besides the dynamics of the airframe and the moving mass, the mass of the air bladder is controlled by another input u_4, as

$$\dot{m}_b = u_4 \tag{6}$$

where m_{b} is the mass of the air bladder.

The full 8-DOF mathematical model of the buoyancy-driven airship is given by Eqs. (3-6). Comparing the modeling in Refs. [9,12], the approach presented here is more clear and simple. It considers the rigid body and the moving mass as two independent parts. Thus, it is possible to refer the modeling of the conventional airship[14-15].

2 CONTROLLER FOR 3-D MOTION

A control scheme based on the singular perturbation for the longitudinal and the lateral dynamics in 3-D space is presented (Fig. 6). Some simulations are does one to show the control performances for the attitude control and the guidance.

Note that the turning direction, namely lateral motion, of the autonomous underwater glider is decided by the roll dynamics, φ and Ω_2, as depicted in Section 1.1. It does not depend on the yaw dynamics, ψ and Ω_3, which are caused by the deflections of the control surface, as it is the case for most underwater and aerial vehicles. Thus, the yaw dynamics, ψ and Ω_3, can be neglected.

2.1 Controller structure

The two-time-scale decomposition of the system model is based on the assumption that the dynamics of the states on the longitudinal plane are slower than those states on lateral plane (Fig. 6). Here, the longitudinal states consist of θ, Ω_2, v_1, v_3, r_{p1}, and $\dot{r}_{p1}$, and the lateral states consist of φ, Ω_1, v_2, v_3, r_{p2}, and $\dot{r}_{p2}$. The yaw states, ψ and Ω_3, are not involved in this decomposition. It is shown a posteriori that this time scale decomposition will be the key for a successful 3-D control.

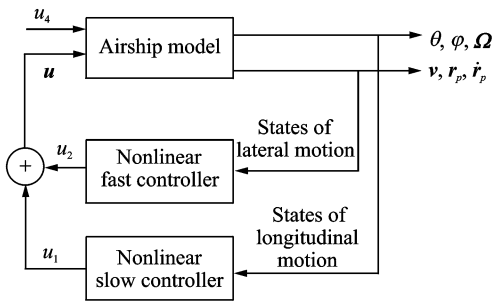

Fig. 6 Structure of singular perturbation controller

The design of the controller is separated into two steps relating to the slow and the fast dynamics.

Even though the full system is reduced into two-time-scale subsystem to design controllers, it is not easy to analyze these subsystem dynamics due to complex nonlinear properties of the system. For a similar mechanism system, PID, LQR, and Lypunov approaches are used to design the controller[9,12] for planar dynamics. Next, a maximal feedback linearization[21-22] approach is adopted to derive a control scheme for 3-D motion.

2.2 Slow dynamics controller

Design of the controller u_1 for slow dynamics shown in Fig. 6 deals with all dynamics in the longitudinal plane. First, rewrite the longitudinal model as

$$\begin{cases} \dot{\theta} = \Omega_2 \\ \dot{\Omega}_2 = \dfrac{1}{J_2}(M_{\mathrm{a}} + r_{p1}u_3 - r_{p3}u_1) \\ \dot{v}_1 = \dfrac{1}{m_1}((\overline{m} - m_0)g\sin\theta - m_3 v_3 \Omega_2 + F_{\mathrm{a}1} - u_1) \\ \dot{v}_3 = \dfrac{1}{m_3}(-(\overline{m} - m_0)g\cos\theta + m_1 v_1 \Omega_2 + F_{\mathrm{a}3} - u_3) \\ \ddot{r}_{p1} = -\dot{v}_1 - \dot{\Omega}_2 r_{p3} - (v_3 - \Omega_2 r_{p1})\Omega_2 - g\sin\theta + u_1/\overline{m} \\ \dot{m}_0 = u_4 \end{cases} \tag{7}$$

where u_3 is not a control input and is decided by Eq. (3) since $\dot{r}_{p3} = 0$ and $\ddot{r}_{p3} = 0$, and the term

$(m_1-m_3)v_1 v_3$ in right side of $\dot{\Omega}_2$ is neglected since it is included in the aerodynamic moment $\boldsymbol{M}_a$[23].

It is difficult to handle subsystem Eq. (7) directly. But a simplified model can provide a great deal of insight into stability and control design. As done in Ref. [13], the complex airship model is simplified into a prismatic-joint pendulum. For completeness, recall the main features.

It is clear that the dynamics in the longitudinal plane is impacted by the following four parts:

(1) The moving mass p_1 which controls the pitch angle θ;

(2) The net lift $m_0 g$ which controls the ascent and the descend of the airship;

(3) The inertial force which is denoted by added masses m_{ii};

(4) The aerodynamic force $\boldsymbol{F}_a$ and $\boldsymbol{M}_a$.

Assume that the airship is fixed at point O and is only subject to the motion of the moving mass to control the pitch angle, and there is no other force affecting the airship. In this situation, the system can be maximally simplified, and the airship rotates around the center of the volume O, which yields the system to be a prismatic-joint pendulum described in Fig. 7. The rotational joint at the point O is not actuated. The joint between the two links of the pendulum is prismatic and actuated. This pendulum, inverted or not, has been considered as a standard control example in many references[24].

The mathematical model for this special case is easy to derive, and it is a subsystem of Eq. (7). An analysis of maximal feedback linearization is done. It is found that there exists an out-put function involving the angular momentum

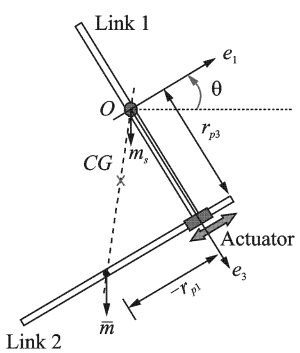

Fig. 7 Simplified airship system identical to prismatic-joint pendulum

of the system around O, which has relative degree 3 and which yields an asymptotically stable zero dynamics.

It is shown that the angular momentum of the system has its relative degree unchanged when more force act on the airship. The angular momentum Π_1 for model Eq. (7) is

$$\Pi_1 = J_2\dot{\theta} + \frac{\bar{m}m_1}{\bar{m}+m_1}\left(\frac{m_3(m_1+\bar{m})}{m_1(m_3+\bar{m})}r_{p1}^2\,\dot{\theta} + r_{p3}^2\,\dot{\theta} + r_{p3}\dot{r}_{p1}\right)$$

Up to some integrating function ρ, the angular momentum Π_1 can be integrated. More precisely, there exists Π_2

$$\dot{\Pi}_2 = \rho\Pi_1 \qquad \rho > 0$$

$$\Pi_2 = \theta + \frac{r_{p3}}{\sqrt{\dfrac{m_3(m_1+\bar{m})}{m_1(m_3+\bar{m})}}\sqrt{\dfrac{\bar{m}m_1}{\bar{m}+m_1}J_2 + r_{p3}^2}} \cdot \arctan\frac{\sqrt{\dfrac{m_3(m_1+\bar{m})}{m_1(m_3+\bar{m})}}r_{p1}}{\sqrt{\dfrac{\bar{m}m_1}{\bar{m}+m_1}J_2 + r_{p3}^2}}$$

Any combination of Π_1 and Π_2 has relative degree 3 and its feedback linearization will yield a linear controllable 3-D subsystem with a 3-D zero dynamics[25]. The following result shows the possibility to ensure that the system is the minimum phase which has a decisive impact on its internal stability and the doability of this control design.

Theorem[13] $y = \Pi_1 + q\,\Pi_2$ has stable zero dynamics for $q > 0$.

For $q>0$, the system is asymptotically stable as ρ is strictly positive and bounded.

From this Theorem, it is mandatory to pick $q>0$ to ensure internal stability of the closed loop system. Its actual value is a tuning parameter which influences the velocity of the zero dynamics. The following error equation is considered

$$y^{(3)} + \lambda_2 y^{(2)} + \lambda_1 y^{(1)} + \lambda_0(y - y_e) = 0 \quad (8)$$

where $y^{(3)}$ is an explicit function of the control input u_1. Thus, Eq. (8) is solved in u_1 and u_1 is embodied static as the state feedback which is computed explicitly after some lengthy but straight forward computations.

2.3 Fast dynamics controller

Design of the controller u_2 corresponding to the fast dynamics in Fig. 6 deals with the states in the lateral plane. The mathematical model for the fast dynamics is derived by letting longitudinal states equal zero

$$\begin{cases}\dot{\varphi}=\Omega_1\\ \dot{\Omega}_1=\dfrac{1}{J_1}(L_a-r_{p2}u_3+r_{p3}u_2)\\ \dot{v}_2=\dfrac{1}{m_2}((m_0-\overline{m})g\sin\varphi+m_3v_3\,\Omega_1+\\ \qquad F_{a2}-u_2)\\ \dot{v}_3=\dfrac{1}{m_3}((m_0-\overline{m})g\cos\varphi+m_2v_2\,\Omega_1+\\ \qquad F_{a3}-u_3)\\ \ddot{r}_{p2}=-\dot{v}_2+\dot{\Omega}_1r_{p3}+(v_3+\Omega_1r_{p2})\,\Omega_2+\\ \qquad g\sin\varphi+u_2/\overline{m}\\ \dot{m}_0=u_4\end{cases}\tag{9}$$

where u_3 is also decided by Eq. (3).

For the fast dynamics controller design, note that the analysis of the slow subsystem remains instrumental. Actually, the lateral controller design is the same as in the longitudinal controller design. This remark is easy to understand when taking into account of the real physical system (Figs. 2-3). The dynamics in the lateral phase has the same structure as the dynamics in the vertical phase, however the parameters are different.

Two moving masses located in two planes respectively, which lead the dynamics in these two planes are identical. The angular momentum for the lateral plane is

$$\Xi_1=J_1\dot{\varphi}+\frac{mm_3}{m+m_3}r_{p2}^2\,\dot{\varphi}-\frac{mm_2}{m+m_2}(r_{p3}\dot{r}_{p2}-r_{p3}^2\,\dot{\varphi})$$

and there exist two functions Ξ_2 and ρ'

$$\dot{\Xi}_2=\rho'\Xi_1\qquad\rho'>0$$

$$\Xi_2=\varphi-\frac{r_{p3}}{\sqrt{\dfrac{m_3(m_2+\overline{m})}{m_2(m_3+\overline{m})}}\sqrt{\dfrac{\overline{m}+m_2}{\overline{m}m_2}J_1+r_{p3}^2}}\cdot\arctan\frac{\sqrt{\dfrac{m_3(m_2+\overline{m})}{m_2(m_3+\overline{m})}}r_{p2}}{\sqrt{\dfrac{\overline{m}+m_2}{\overline{m}m_2}J_1+r_{p3}^2}}$$

Ξ_1 and Ξ_2 have relative degree 3. By the same way, it is easy to prove that $y'=\Xi_1+q'\Xi_2$ has stable zero dynamics for any $q'>0$. An error equation as Eq. (8)

$$y'^{(3)}+\lambda_2'y'^{(2)}+\lambda_1'y'^{(1)}+\lambda_0'(y'-y_c')=0\tag{10}$$

is adopted to design controller u_2 to stabilize the flight path angle γ and speed to commands in the lateral plane. The parameters of the controller are represented by λ_2', λ_1', and λ_0'. The exact expression of u_2 is easily computable, although through tedious computations. Similar simulation results as that for the longitudinal dynamics are obtained for the dynamics in the lateral plane.

3 SIMULATIONS OF NOMINAL CONTROL RESPONSES

Through the simulation in 3-D space, it is found that if six poles of the error Eqs. (8,10) are all arranged at the same places, namely $\lambda_i=\lambda_i'$, then the controllers u_1 and u_2 are too large and exceed an acceptable domain. When the longitudinal dynamics is slow and the lateral dynamics is fast, the magnitudes of u_1 and u_2 are acceptable. This also shows the necessity of a singular perturbation approach. In this paper, the following values are chosen: $q=q'=50$, $\lambda_2=3$, $\lambda_1=3$, $\lambda_0=1$, $\lambda_2'=30$, $\lambda_1'=300$, and $\lambda_0'=1\,000$.

The superposition of both actions of controllers are applied to the nonlinear coupled full model Eqs. (3-5). All mechanical properties used in the simulation are listed in Table 1.

Table 1 Physical properties of airship

Term	Value	Term	Value
$\overline{m}$/kg	30	Volume/m^3	296
m_s/kg	269	m_1/kg	400
m_2/kg	400	m_3/kg	500
J_1/(kg·m^2)	9 000	J_2/(kg·m^2)	8 000
J_3/(kg·m^2)	3 000	r_{p3}/m	2

Two simulations are done to present the performance of the control scheme in Section 2. The first simulation presents a typical turning case in 3-D space. Finally, the second simulation presents a continuing flight which includes ascent

and descent in 3-D space. The values used in these simulations are collected in Table 2.

Table 2 Specified flight paths and commands

Term	Path 1	Path 2	Term	Path 1	Path 2
$V_e/(\mathrm{m}\cdot\mathrm{s}^{-1})$	10	10	m_0/kg	−6.2	−6.2
$\xi_e/(°)$	29.2	31.7	k	50	50
$\gamma_e/(°)$	0	−10	λ_2	3	3
$\theta_e/(°)$	20	20	λ_1	3	3
$\varphi_e/(°)$	0	15	λ_0	1	1
r_{p1e}/m	−0.74	−0.74	λ_2'	30	30
r_{p2e}/m	0	0.53	λ_1'	300	300
$v_{1e}/(\mathrm{m}\cdot\mathrm{s}^{-1})$	9.9	9.7	λ_0'	1 000	1 000
$v_{2e}/(\mathrm{m}\cdot\mathrm{s}^{-1})$	0	−2.1	$v_{3e}/(\mathrm{m}\cdot\mathrm{s}^{-1})$	−1.6	−1.5

(1) Turning case

The first simulation, as shown in Figs. 8-13, presents a typical turning case for the airship, which means that the airship firstly ascends in the longitudinal plane, and then turns to $-j$ direction. Here it simulates a combined situation of the first two simple cases.

The reference direction and speed of the trajectory, the commands of the states, and the parameters of the second simulation are specified by Path 1 and Path 2 in Table 2. As shown in Figs. 8-9, the motion of the airship is restricted on the longitudinal plane in the the first 100 s. After that, the airship is controlled to turn right to follow a flight path angle $\gamma=10°$.

The simulation is to show the performance of the controller in a typical turning case. Actually, during this turning case, the system transfers from a 2-D case[13] to a 3-D case.

From the actual values of ξ, γ, and V presented in Fig. 10, good tracking performance of the controller are shown. Comparing the dynamics of the longitudinal motion (consists of θ, r_{p1}, and u_1) and the lateral motion (consists of φ, r_{p2}, and u_2) in Figs. 11-13, it is easy to find that the interaction between these two planes is weak since when the lateral states transfer from zero to the commands, the longitudinal states keep stable.

(2)Continuing flight in 3-D space

Fig. 14 shows a flight which consists of ascent and descent in 3 - D space . The goal of this

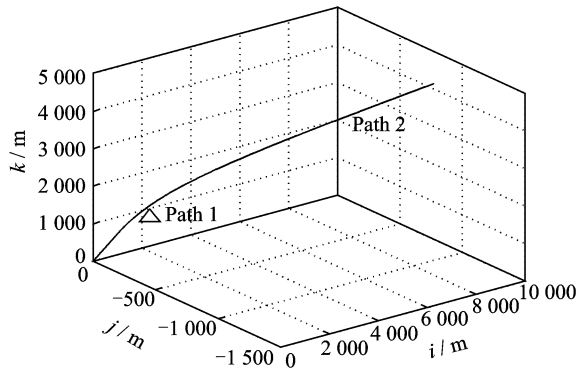

Fig. 8 Moving trajectory in 3-D space

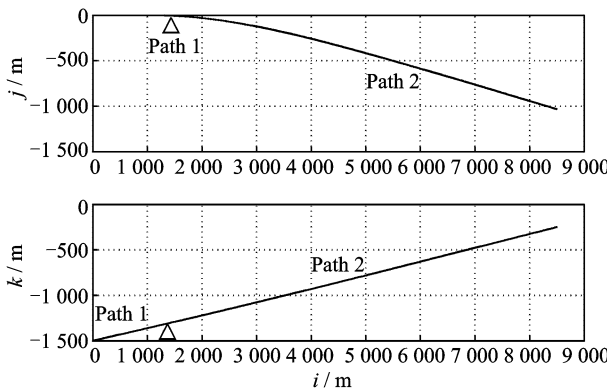

Fig. 9 According trajectories in 2-D space

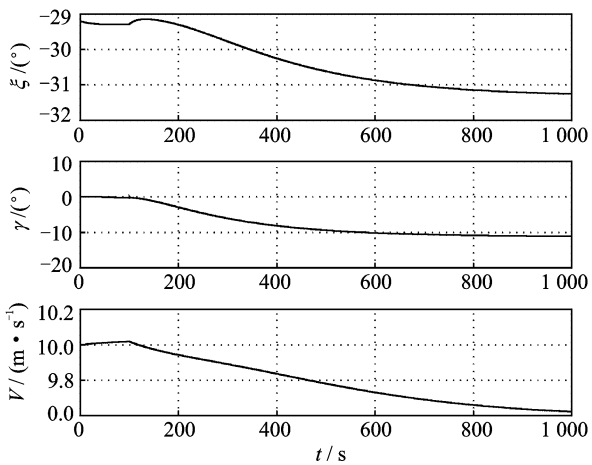

Fig. 10 Actual values of flight path angles ξ, γ and speed V

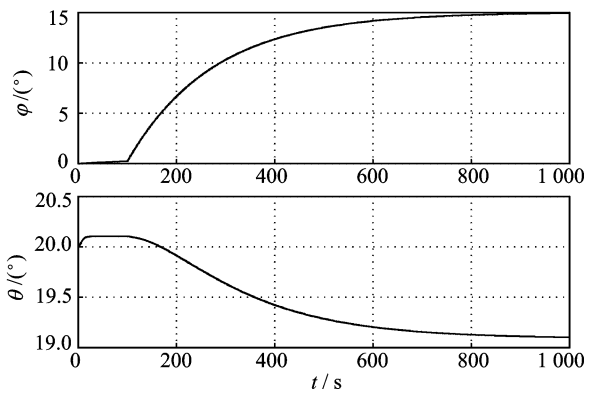

Fig. 11 Dynamics of attitude φ and θ

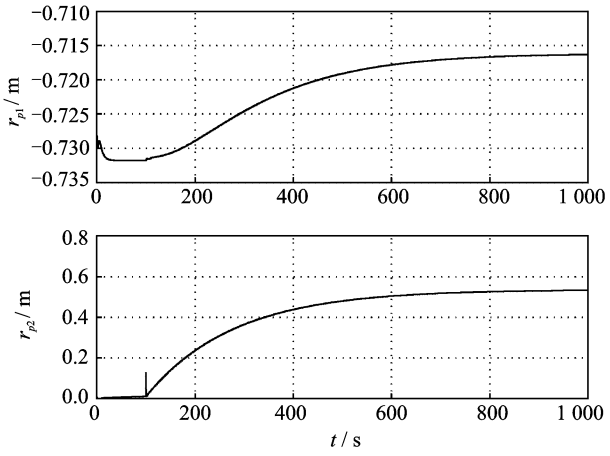

Fig. 12 Motions of moving masses

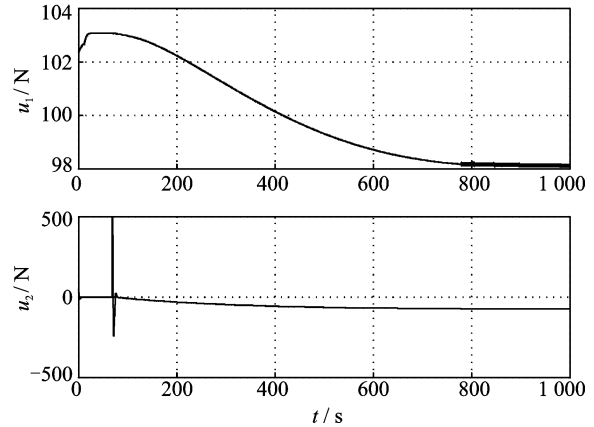

Fig. 13 Dynamics of control

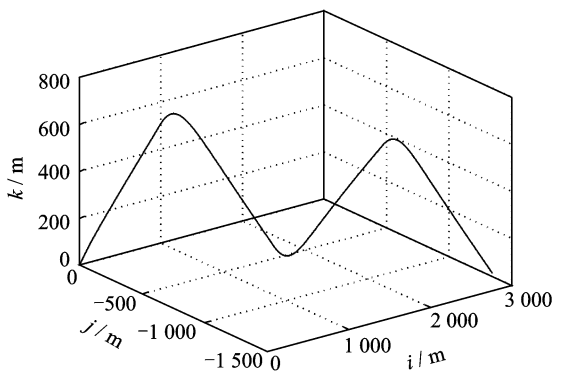

Fig. 14 Trajectory for continuing turning flight in inertial frame $G\{i, j, k\}$

simulation is to shown this controller can continually cover the transition points and keep stable to track reference trajectories in 3-D space.

4 CONCLUSIONS

The buoyancy-driven airship which employs internal moving mass to control the attitude and adjustable internal air bladder to control the altitude offers a novel mechanism for UAVs. This driving mechanism is more complicated than conventional airships due to the existence of the internal dynamics and special buoyancy propeller. This paper views the internal moving masses and the rigid body as two independent parts, which simplified the modeling and makes it more clear.

To present, the discussion on the control of this mechanical system is mainly limited to one plane (i. e., the longitudinal plane) and linear controllers. Through a singular perturbation scheme, a nonlinear feedback control scheme for the 3-D attitude control problem and the guidance problem are derived for the first time. With the controller proposed here, not only the longitudinal dynamics can be stabilized, but also steady turning direction can be achieved by the feedback u_2. The control performance of this control approach for dynamics in 3-D space is acceptable. The result of this paper is useful for similar mechanical systems, such as underwater gliders and re-entry vehicles.

Obviously, severe wind conditions are not considered here, and they may give the limits of the airship design and the minimal use of standard propulsion may become mandatory and requires further investigations.

References:

[1] Tozer T C, Grace D. High-altitude platforms for wireless communications[J]. IEEE Electronics and Communications Engineering Journal, 2001,13(3): 127-137.

[2] Bowes W C, Engelland J, Fernandez F L, et al. Lighter-than-air systems for future naval missions [R]. Virginia, USA: Naval Research Advisory Committee Arlington Va, 2006.

[3] Lindstrand P. ESA-HALE airship research and development program[C]//The 2nd Stratospheric Platform Systems Workshop. Tokyo, Japan: [s. n.], 2000:15-21.

[4] Grace D, Mohorcic M, Horwath J, et al. Communications from aerial platform networks delivering broadband for all—An overview of the CAPANINA project[C]//Invited Paper for Korean Workshop on HAPs. Seoul, Korea: [s. n.], 2004: 1-12.

[5] Knaupp W, Mundschau E. Solar electric energy supply at high altitude[J]. Aerospace Science and Technology, 2004,8: 245-254.

[6] Yokomaku Y. Current progress in the SPF airship

R&D program of Japan[C] //The 3rd Stratospheric Platform Systems Workshop. Tokyo, Japan: [s. n.], 2001: 15-19.

[7] Purandare R Y. A buoyancy-propelled airship[D]. Las Cruces, USA: Engineering College, New Mexico State University, 2007.

[8] Stommel H. The slocum mission[J]. Oceanography, 1989, 2(1): 22-25.

[9] Leonard N E, Graver J. Model-based feedback control of autonomous underwater gliders[J]. IEEE Journal of Oceanic Engineering, 2001, 26(4): 633-645.

[10] Webb D C, Simonetti P J, Jones C P. SLOCUM, an underwater glider propelled by environmental energy [J]. IEEE Journal of Oceanic Engineering, Special Issue on Autonomous Ocean Sampling Networks, 2001, 26(4): 447-452.

[11] Sherman J, Davis R E, Owens W B, et al. The autonomous underwater glider 'Spray' [J]. IEEE Journal of Oceanic Engineering, Special Issue on Autonomous Ocean Sampling Networks, 2001, 26(4): 437-446.

[12] Bhatta P. Nonlinear stability and control of gliding vehicles[D]. New Jersey, USA: Department of Mechanical and Aerospace Engineering Princeton University, 2006.

[13] Wu X, Moog H. C, Marquez-Martinez L A, et al. Modelling and Control of a Complex Buoyancy-Driven Airship[C]//8th IFAC Symposium on Nonlinear Control Systems. Italy: University of Bologna, 2010: 55-59.

[14] Gomes S B V, Ramos J Jr G. Airship dynamic modeling for autonomous operation[C]//IEEE Int Conf on Robotics and Automation. Leuven, Belgium: IEEE, 1998: 3462-3467.

[15] Mueller J B, Paluszek M A, Zhao Y. Development of an aerodynamic model and control law design for a high altitude airship[C]//AIAA 3rd Unmanned U-Mimited Technical Conference. Chicago, USA: [s. n.], 2004: 121-126.

[16] Petsopoulos T, Regan F J, Barlow J. Moving-mass roll control system for fixed-trim re-entry vehicle [J]. Journal of Spacecraft and Rockets, 1996, 33 (1): 54-60.

[17] Naidu D S, Calise A J. Singular perturbations and time scales in guidance and control of aerospace systems: A survey[J]. Journal of Guidance Control and Dynamics, 2001, 24(6): 1057-1078.

[18] Thomasson P G. Equations of motion of a vehicle in a moving fluid[J]. Journal of Aircraft, 2000, 37: 630-639.

[19] Lamb H. The inertia coefficients of an ellipsoid moving in fluid[R]. London: British Aeronautical Research Committee Report and Memoranda, 1918.

[20] Munk M M. Aerodynamics of airships[J]. Aerodynamics Theory, 1936, 6: 36-45.

[21] Isidori A. Nonlinear control systems: an introduction[M]. the 2nd Edition. NY: Springer, 1989.

[22] Conte G, Moog H C. Perdon A M. Algebraic methods for nonlinear control systems-theory and applications [M]. the 2nd Edition. London: Springer, 2007.

[23] Ouyang J. Research on modeling and control of an unmanned airship[D]. Shanghai: Shanghai Jiaotong University, 2003. (in Chinese)

[24] Wie B. Space Vehicle dynamics and control[M]. Reston, USA: AIAA, 1998.

[25] Isidori A, Moog. H. C. On the nonlinear equivalent of the notion of transmission zeros[C]//Workshop on Modelling and Adaptive Control. Sopron, Hungary, Berlin, German: [s. n.], 1986, 105: 445-471.

浮力驱动飞艇在三维空间中一种基于奇摄动理论的移动质量块控制方法

吴小涛[1,2] Claude H Moog[2] 胡跃明[1]

(1. 华南理工大学自动化学院, 广州, 510640, 中国; 2. 法国南特通信与控制研究所, 南特, 44321, 法国)

摘要: 对浮力驱动飞艇在三维空间中的姿态和航向控制提出了一种解决方法。介绍了建立该飞艇八自由度数学模型的方法。基于最大反馈线性化方法推导了纵向平面和侧向平面的非线性反馈控制, 证明了内部的动态稳定性。通过奇摄动理论叠加在两个平面的控制, 推导出一种三维运动控制方法。基于该控制方法, 对飞艇跟踪指定姿态, 航向和速度进行了仿真。

关键词: 浮力驱动; 飞艇; 非线性控制; 三维; 奇摄动

中图分类号: TP2; V1

(Executive editor: Sun Jing)

基金项目: 中国留学基金委员会公派留学基金资助项目。